Mechanical and Finite Element Analysis of an Innovative Orthopedic Implant Designed to Increase the Weight Carrying Ability of the Femur and Reduce Frictional Forces on an Amputee's Stump

Tejas P. Chillale; Nam Ho Kim*; Larry N. Smith†*

ABSTRACT This study was designed to test the hypothesis that: "*A properly designed implant that harnesses the principle of the incompressibility of fluids can improve the weight carrying ability of an amputee's residual femur and reduce the frictional forces at the stump external socket interface*." The hypothesis was tested both mechanically on an Amputee Simulation Device (ASD) and through Finite Element Analysis (FEA) modeling software. With the implant attached to the femur, the FEA and ASD demonstrated that the femur carried 90% and 93% respectively of the force of walking. Without the implant, the FEA model and ASD femur carried only 35% and 77%, respectively, of the force of walking. Statistical calculations reveal three (3) degrees of separation (99% probability of non-random significant difference) between with and without implant data points. FEA modeling demonstrates that the normal contact forces and shear forces are pushed the distal weight-bearing area of the amputee stump, relieving the lateral stump of frictional forces. The ASD mechanical and FEA modeling data validate each other with both systems supporting the hypotheses with confidence intervals of three degrees of separation between with implant and without implant models.

INTRODUCTION

A lower limb amputation has a devastating impact on an individual's quality of life. Amputees can use an external walking prosthetic but many have a less than satisfactory experience with the use of this prosthesis. A substantial number of amputees report stump skin irritation, skin ulceration, pain with walking, ambulatory difficulty, diffuse musculoskeletal pain, difficulty standing for extended periods and fatigue. Due to this, 40% of amputees cannot use their prosthetic periodically and 25% choose not to use the external prosthetic at all.[1–9]

This study tests the experimental efficacy of an implant (Fig. 1) that is fixed to the cut end of the bone and designed to enhance the amputee's stump-socket interface utilizing the principle of fluid incompressibility.[10] The device utilizes the 60% of body weight that is water[11] allowing for the transfer of the energy of walking from the external prosthetic through the fluid environment of the skin and soft tissue of the stump concentrating it in the bone. This prosthetic implant can deform its shape when loads are applied in different directions but still transmit the force of walking to the femur. The data presented here support the hypothesis and the experimental efficacy of this unique orthopedic implant.[12–18]

METHODS

The study used real-time physical testing of prototype orthopedic implants on a proprietary amputation simulation device (ASD [patent pending]). The ASD was used to validate the finite element analysis (FEA) testing and demonstrate the efficacy of the prototype implants. Computer simulation was accomplished using a commercially available FEA software program (*Abaqus* – Dassault Systems). To test the hypothesis and the efficacy of the implants these two systems collected data that were used to measure the average input and output force in kilograms (Kg), calculate the ratio of output to input forces, calculate the average force per unit area in Kg/cm^2, calculate the Von Mises stress in the femur, and calculate the effect of the implant on the normal contact forces (NCF) and shear forces on the amputee stump.

Materials

The ASD device was designed and built to simulate an above-the-knee amputation. It allowed for application of force upward through an artificial external walking prosthesis. This force is then absorbed by the simulated amputee stump made of 10% FBI ballistic gel (Clear Ballistics) that simulates tissue. The simulated femur is encased in the ballistic gel with or without the implant prototype attached. Force is applied in a stair step fashion as the sliding force plate moves increasing heights underneath the stump compartment. Input and output forces are measured in a steady

*Department of Mechanical & Aerospace Engineering, 231 MAE-A, P. O. Box 116250, University of Florida, Gainesville, FL 32611-6250.

†M:14;22-33, LLC, 10925 SW 27th Ave Gainesville, FL 32608-8937.

M-14 President and CEO: Larry N. Smith MD. As to conflict of interest, Dr. Smith is the patent holder of the implants and the owner M:14;22–33, LLC. Dr. Smith had no participation in the FEA testing and analysis.

doi: 10.1093/milmed/usy382

© Association of Military Surgeons of the United States 2019. All rights reserved. For permissions, please e-mail: journals.permissions@oup.com.

Downloaded from https://academic.oup.com/milmed/article-abstract/184/supplement_1/627/5418698 by University of Florida user on 02 April 2019

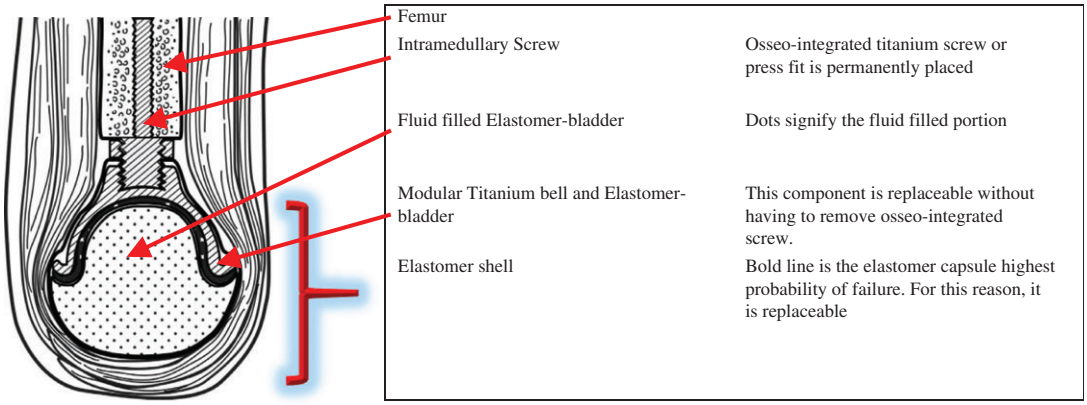

FIGURE 1. Device drawing and legend.

state environment with force sensors (Phidgets). Data are collected in a proprietary data collection software program.

FEA modeling was conducted in a 2D parametric manner to allow for rapid prototype testing, control of computation cycle times and provide data for future 3D modeling. The trend of 2D parametric results was then validated against the ASD measured results. The parameters for FEA modeling and boundary conditions are outlined in Table I.[19–21]

TABLE I. Material Properties of FEA Modeling Material

Material Characterization	Young's Modulus (E)	Poisson' Ratio (ν)
Socket 15.5–21 (GPa)	15.5–21 (GPa)	0.3
Skin 0.1–0.12 (MPa)	0.1–0.12 (MPa)	0.475
Tissue 30 (kPa)	30 (kPa)	0.49
Muscle 0.16 (MPa)	0.16 (MPa)	0.49
Bone 10–15 (GPa)	10–15 (GPa)	0.32
Implant 0.15 (MPa)	0.15 (MPa)	0.492
Above Implant 5.5 (MPa)	5.5 (MPa)	0.38

Properties for the socket and partitions in the stump

METHODS

For the ASD Testing

Two prototype orthopedic implants (5.5 inches, surface area in square inches = 47.53 in^2, surface area in square cm = 306.68 cm^2 and 3.5-inches, surface area in inches = 19.25 in^2, surface area in cm = 124.4 cm^2) were designed and built. The implants' efficacy was tested on an ASD that allows for the application, transfer, and measurement of input and output forces in Kg with force sensors. The input-force (0–200 kg) was applied through the simulated external prosthetic leg with the output forces measured at the stump's implant-femur interface or femur alone interface after diffusion through 10% ballistic gel.

Three test models were used on the ASD. These were Model 1 with the 5.5 inch diameter prototype implant with femur, Model 2 with the 3.5 inch diameter prototype implant with femur and Model 3 with a 1.5 inch (1.5 inch diameter simulated femur, Surface area in inches = 1.7679 in^2, Surface area in square cm = 11.4055 cm^2) diameter femur only.

For Nonlinear 2D FEA Modeling

Commercially available FEA software *Abaqus* produced by Dassault Systems was used to calculate the performance and efficacy of the prototype implant design models versus the femur alone model. The thickness of 2D FEA model was selected such that the total volume of 2D FEA model was representative real 3D volume. All the FEA model simulations were run on a simulated left leg above-knee-amputation. The skin, subcutaneous tissue partitions or layers were assumed to be in 0.8 cm thick inside the stump. The radius for small implant size was taken as 3.5 cm. and radius for larger implant size as 4.5 cm. The 2D modeling was calculated for both sections and plane-strain conditions and applied with a finite element thickness of 11.2 cm.[22–24]

FEA Modeling Design and Rational

The FEA model is composed of socket, skin-tissue-muscle partition, bone and implant. The stump is partitioned into several sections to distinguish skin, subcutaneous tissue, muscle, femur, implant, and implant support. The interface between socket and skin is modeled using frictional contact, while all other interfaces are assumed to be fully connected. All partitions are modeled using four-node quadrilateral plane-strain elements with a finite thickness. After modeling the design of stump and socket for both sections, meshing is done with freely structured 4 node bilinear plane-strain standard quadrilateral elements, CPE4. Each model used linear elastic isotropic property to represent the bone, stump and socket mechanical behavior. The material properties for each partition (layer) are assigned as shown in Table I. The contact interaction condition is allowed with tangential and normal behavior. Isotropic friction conditions was used with a coefficient of friction of 0.7~0.9. The force weight load (78 Kg) is applied in the vertical positive "y" direction as shown in Figure 2A and B. The weight load is applied on

Downloaded from https://academic.oup.com/milmed/article-abstract/184/supplement_1/627/5418698 by University of Florida user on 02 April 2019

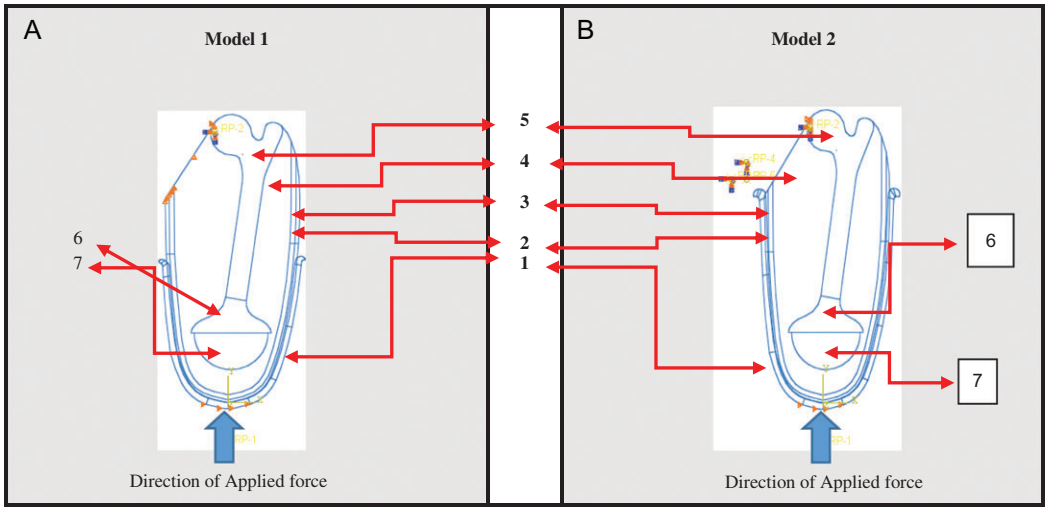

FIGURE 2. (A) Model 1 general limb-socket model example of left above knee stump and socket, with implant used below femur:*1 – socket, *2 – stump skin partition, *3 – stump tissue partition, *4 – stump muscle partition, *5 – stump femur/bone partition, *6 – stump implant partition, *7 – stump above implant partition (material connecting implant and femur), (B) Model 2 limb-socket model example of left above knee stump and socket (in contact with lower region of pelvic bone), with implant used below femur: *1 – socket in contact with pelvic bone (contact in top left), *2 – stump skin partition, *3 – stump tissue partition, *4 – stump muscle partition, *5 – stump femur/bone partition, *6 – stump implant partition, *7 – stump above implant partition (material connecting implant and femur).

the reference point, which is away from the socket in same direction of load, then transmitted to the socket using distributed coupling constraint. For the load and boundary conditions, the top point of the femur in the design is assumed to be in contact with the hip joint which restricts its vertical and horizontal movement. This point acts as a pivot for rotation of femur along *X-Y* plane. This point also has spring boundary condition (spring constant = 38,415 N/m) along *Z* direction which allows the femur to rotate only up to 2–3 degree angle in anticlockwise direction. The bottom most point of the socket is fixed in the *Y* and *Z* directions. The load applied on the socket is a result of the remaining prosthesis (shaft) which is attached between socket and the ground. For Model 2, an additional boundary condition is set in which there is restriction in the left topmost part of the socket due to its approximation to the ischial tuberosity. Spring boundary conditions are applied to this point, which restrict socket movement to about 2 ~ 3 cm in vertical/horizontal direction. In both models, there is restricted boundary condition for the proximal region between the ischial tuberosity and the restricted femur point in contact with hip joint. This is assumed due to unknown factors causing less movement or restriction through the inner section of pelvis.[25–34]

Two different simulation models based on the external socket design with four subsets each were considered in 2D FEA computational analysis. Model 1 had no socket contact below or with the Ischial Tuberosity (IT) of the Pelvis (Fig. 2 Model 1). The Model 1 socket had a top opening diameter of 12.5 cm and length of 15.5 cm. Model 2 had the proximal medial edge of the socket in contact with the IT on the Pelvis (Fig. 2 Model 2). The Model 2 socket had a length and top opening diameter as 25 cm and 15 cm, respectively. Model 1 and 2 had four subset designs named Model 1 or 2 – "a" – residual femur only, "b" – 3.5 cm radius implant, "c" – 4.5 cm radius implant, or "d" – 4.5 cm radius implant adjacent to skin surface (Fig. 3"a"–"d"). Design "a" represented the conventional configuration of low-limb amputation, and other designs have the proposed implantable device with different sizes. Design "a" is used for a reference in a comparative study using FEA.

Von Mises stresses were calculated to understand the load path. The total vertical shear force due to contact was calculated on the stump to observe the amount of weight/force load transmitted or applied through the skin. Profiling of NCF and resultant shear forces was utilized for comparison in the different designs of respective models.

FEA Model-2 calculated the reaction force near the IT due to the restricted socket movement at that point and the reaction force at the restricted femur point in contact with hip joint.

In order to apply a point load, a reference point was created below the socket, and made a distributed coupling constraint with the bottom portion of the socket (Fig. 2A and B). A load corresponding to the weight of a human to the reference point (78 Kg) was then applied there. This load will then be distributed to the bottom portion of the socket without causing any stress concentration.

For a given model, the same boundary conditions are used for all different cases. Therefore, the relative comparisons are independent of boundary conditions. However, for Model 2, the changes in outcome are a direct result of the changes in the boundary conditions from Model 1 as noted above. This is very similar to the mechanically dysfunctional

Downloaded from https://academic.oup.com/milmed/article-abstract/184/supplement_1/627/5418698 by University of Florida user on 02 April 2019

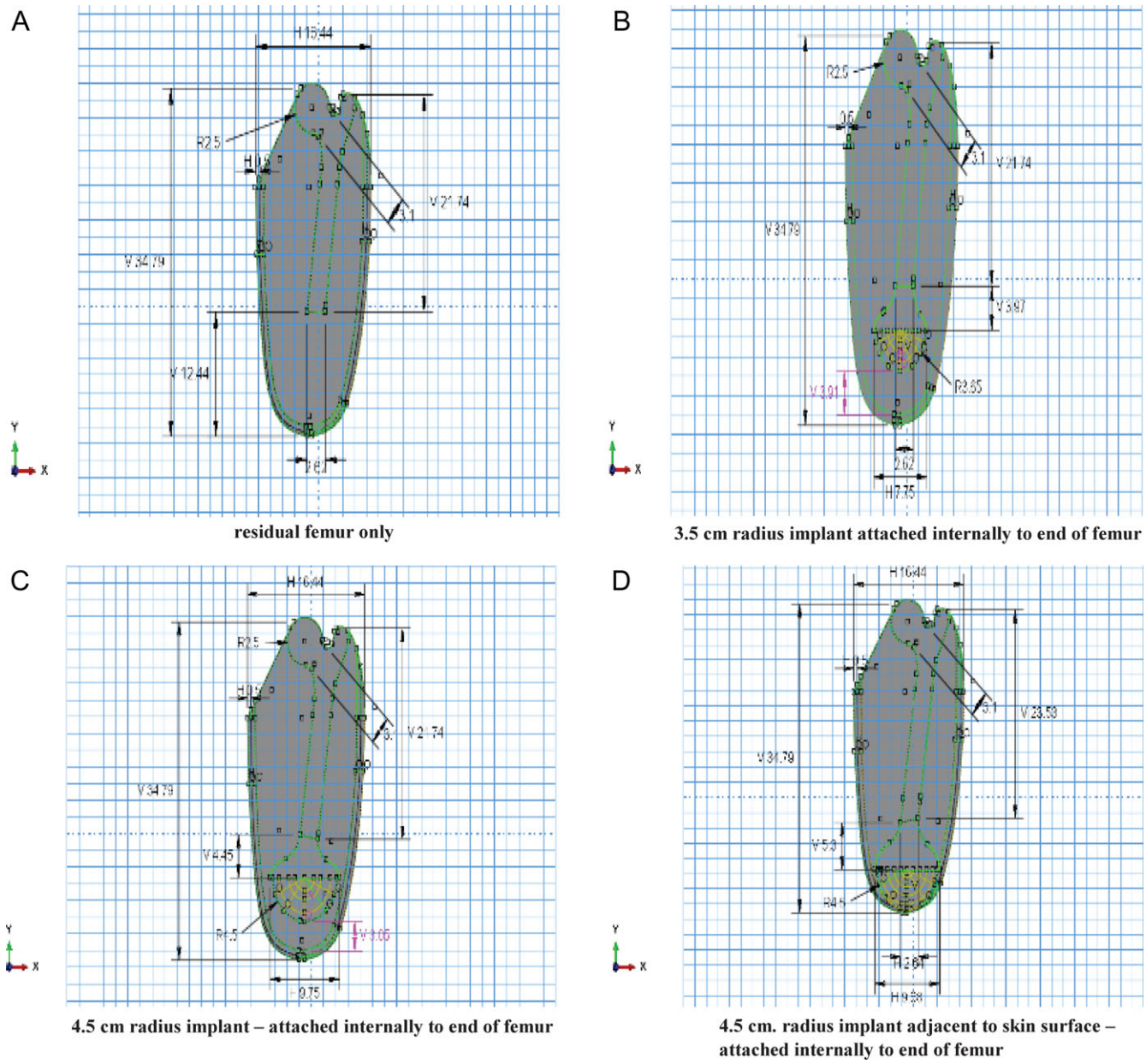

FIGURE 3. Graphic renditions of models used in FEA Modeling and experimental testing Model "a" Femur only with 1.5 cm surface area with 12.44 cm separation distance from distal skin prosthetic interface. Model "b" 3.5 cm diameter implant with 3.91 cm separation distance from distal skin prosthetic interface. Model "c" 4.5 cm diameter implant with 3.0 cm separation distance from distal skin prosthetic interface. Model "d" 4.5 cm diameter implant with subcutaneous tissue and skin barrier only between implant and external prosthetic interface.

sockets that amputee's use daily that prevent the residual femur to carry more if any additional force.

FEA Model-1 and Model-2 Subtype "d"

The FEA Model-1 and Model-2, sub-model "d" was a design to assess the ability of the implant to absorb and transmit force through limited tissue and in near direct contact with the external prosthetic (Figs 3D, 5D, and 6D). This model was tested on the ASD platform to validate the FEA modeling design.

RESULTS

For ASD Testing

Output/Input Ratios (O/I Ratios)

The Model-1 5.5 inch diameter implant had an average maximum O/I ratio of 0.93 ± 0.0063 (93 ± 0.63%) calculated from four separate runs on the ASD. Model-2's 3.5 inch diameter implant had an average maximum O/I ratio was 0.86 ± 0.0073 (86 ± 0.73%). Model-3's 1.5 inch diameter femur only model had a maximum O/I force ratio transfer of 0.7361 ± 0.955 (73.61 ± 0.955%) (Table IIA and Fig. 7).

Downloaded from https://academic.oup.com/milmed/article-abstract/184/supplement_1/627/5418698 by University of Florida user on 02 April 2019

Model 1 and 2 Subtype "d" demonstrated the highest output/input ratios with over 95% transfer of the applied force on FEA and ASD testing. The force per unit area was similar to the ASD 5.5 cm implant with marked reduction in force per unit area. These data also validated the FEA modeling results (Table IIA and Fig. 7).

Force per Unit Area

Force per unit area calculations demonstrated that the Model-1 5.5 inch implant had the lowest force per unit area of 0.394 Kg/cm^2 compared to the femur alone Model-3 with 9.272 Kg/cm^2. The 3.5 inch Model-2 demonstrated an intermediate force per unit area value of 0.99 Kg/cm^2 (Table IIB and Figure 8). The femur alone model had 23.5 times and 9.34 times the force per unit area than did the 5.5 implant and 3.5 inch diameter implants respectively. The ASD Model 4-"d" design with the implant resting against the skin external prosthetic interface demonstrated force per unit area values similar to FEA modeling and the 5.5 cm implant (Table IIB and Fig. 8).

TABLE IIA. O/I Ratios for All ASD Tuns

Summary Force Output/Input Ratios			
Force Level	5.5 cm O/I Ratios	3.5 cm O/I Ratios	1.5 cm O/I Ratios
1	0.68	0.71	0.56
2	0.85	0.81	0.68
3	0.90	0.84	0.73
4	0.93	0.87	0.77

This table shows the average force output/input ratios for all runs for the two implant sizes and femur alone runs. Force level 4 data is for maximum force input with the maximum output force ratios demonstrating the 5.5 inch implant is capable of transferring 0.93 or 93% of the applied force to the femur/hip joint. There are three sigma of separation between the implant models and the femur only models. See Figure 7 and Table V.

TABLE IIB. Force per Unit Area for All ASD Runs Kg/cm^2

Average of All Runs			
$P = F/A$ units Kg/cm^2			
Force Level	5.5 cm in Implant F/A	3.5 cm in Implant F/A	1.5 cm Femur F/A
1	0.0623	0.314	3.227
2	0.156	0.553	5.582
3	0.266	0.744	7.432
4	0.395	0.992	9.272

This table shows the average force per unit area calculations based on output force divided by area of absorption for all runs for the two implant sizes and femur alone runs. Level 4 data is for maximum force input with the output force demonstrating the 5.5 inch implant is capable of transferring 0.93 or 93% of the applied force to the femur/hip joint with a maximum of 0.395 Kg/cm^2 which is 23.5 times smaller F/A than femur alone model which is 9.27 Kg/cm^2. See Figure 8.

For the FEA Modeling

Shear Forces and NCF

The NCF and the total vertical shear forces at the restricted boundary conditions for each section are displayed in Tables IIIA and IIIB and Tables IVA and IVB, respectively. Tables IIIA and IIIB provide a quantification on the amount of weight load transferred through the skin of the stump and

TABLE IIIA. FEA Net Reaction Force (in Kg) for Designs of Both Models at Respective Contact Points

Net Reaction Forces in Kg					
FEA Socket Model Number See Fig (1)		FEA Model Subset See Fig (2))			
		a	b	c	d
1	on *HJC	68.83	72.14	72.754	73.23
2	on *HJC	49.72	53.6	55.36	61.11
2	on **SPC	25.18	20.4	19.59	13.75

*HJC: hip joint contact. **SPC: socket-pelvic bone contact.

TABLE IIIB. Net Vertical Shear Force (in Kg) on Skin Surface of the Stump For Respective Designs in Both Models

Shear Forces (Kg)				
FEA Socket Model Number (See Fig. 1)	FEA Sub-model Design (See Fig. 2)			
	a	b	c	d
1	3.1	0.01	−0.3	−6.32
2	−4.1	−4.27	−3.57	−8.91

TABLE IVA. Models 1 and 2, Subtypes "a", "b", "c", and "d": Average and Maximum (N) Values of Resultant Shear Forces for Each Sub-design of Both Models

FEA Shear Forces in Newton's (N)								
	Model 1 Sub-model				Model 2 Sub-model			
Shear (N)	"a"	"b"	"c"	"d"	"a"	"b"	"c"	"d"
Average	0.44	0.38	0.39	0.45	0.63	0.76	0.72	0.58
Maximum	3.11	2.69	2.63	2.65	3.25	2.71	2.77	2.86

TABLE IVB. Models 1 and 2, Subtypes "a", "b", "c", and "d": Maximum and Average Values of Normal Contact Forces (NCF) for Each Sub-design of Both Models

FEA Normal Contact Forces in Newton's (N)								
	Model 1 Sub-model				Model 2 Sub-model			
NCF (N)	"a"	"b"	"c"	"d"	"a"	"b"	"c"	"d"
Average	14.07	16.16	16.22	18.89	9.74	9.7	9.94	13.47
Maximum	17.99	20.4	19.1	23.2	17.54	13.64	13.92	17.65

Downloaded from https://academic.oup.com/milmed/article-abstract/184/supplement_1/627/5418698 by University of Florida user on 02 April 2019

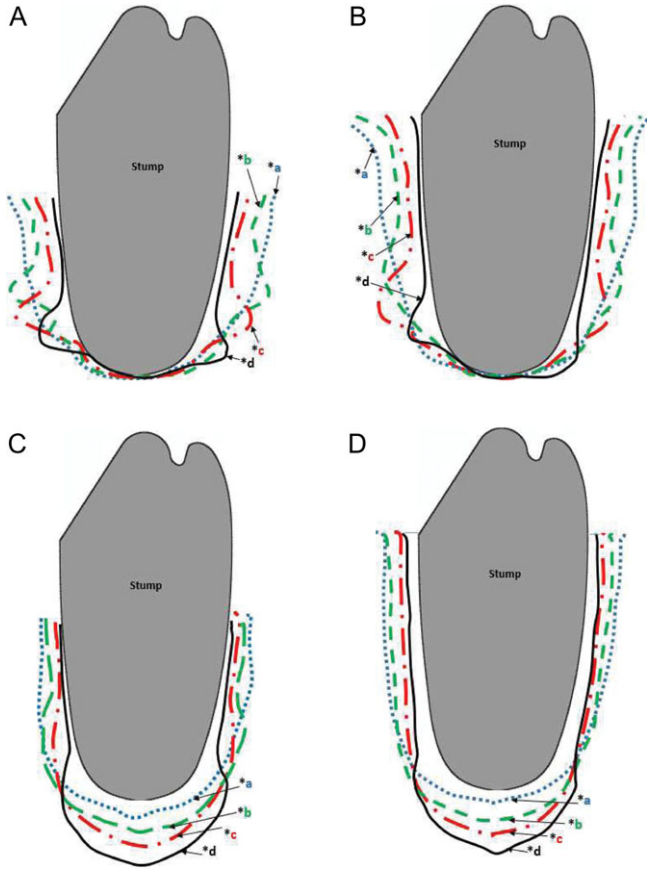

FIGURE 4. The normal contact forces were acquired as output from FEA in Abaqus. This profiling provides a sense of localization for normal contact forces with its magnitude. The maximum and average of resultant sheer forces and normal contact forces for individual models in both sections were calculated from output as shown in the Table IVB [part labels (4-1)–(4-4)]. Designs assigned (see Fig. 2)*a = No implant/ femur only, *b = 3.5 cm implant *c = 4.5 cm implant, *d = 4.5 cm implant adjacent to skin surface. Profiles of resultant sheer forces are utilized to display the regions of their action on the stump, for individual designs of respective models (Table IVA). The normal contact forces were acquired as output from FEA in Abaqus. This profiling provides a sense of localization for normal contact forces with its magnitude. The maximum and average of resultant sheer forces and normal contact forces for individual models in both sections were calculated from output as shown in the Tables IVA and IVB.

also the amount actually carried through the femur at the hip joint respectively for both sections. Tables IVA and IVB provide data that profiles the NCF and resultant shear forces. These data are utilized to display the regions of their action on the stump, for individual designs of models "a", "b", "c", and "d" in Figure 4A–D, respectively. This profiling provides a sense of localization for shear and NCF with its magnitude and location.

Von Mises Stress

In the FEA modeling, the Von Mises stress in the femur was quantified and is displayed in Figure 5A–D for Model 1 and Figure 6A–D for Model 2.

In the Model-1 short socket, the FEA Von Mises stress calculations demonstrated forces of 30%, 86%, and 95% and over 95% for the femur alone "a" model, 3.5 cm radius "b" model, 4.5 cm radius "c" model, and 4.5 cm radius "d" model, respectively.

In the Model-2 long socket, the Von Mises's calculations demonstrated the forces of 30%, 83%, 91% and greater than 91% for femur alone "a" model, 3.5 cm radius "b" model, 4.5 cm radius "c" model, and 4.5 cm radius "d" model respectively.

Test Model Comparisons

When comparing the ASD femur O/I ratios to the FEA Von Mises stress ratio calculations, significant correlations are found between the two. The ASD bench-testing demonstrated that the transfer of maximum O/I force to the femur as percentage of input force was 93 ± 0.63, 86 ± 0.73, and 68.86 ± 4.3% for the 5.5-inch, 3.5-inch implants, and 1.5-inch femur alone models, respectively. For the FEA modeling, Von Mises stress calculations demonstrated an average for both models of 93, 84.5 and 30% transfer of the applied force to the femur for the 4.5-cm radius, 3.5 cm radius, and femur alone models, respectively. FEA Model 2 resulted in less force being carried by the femur because of the fixation point at the pelvis. Regardless, with the implant present the femur carried three (3) degrees of separation of force load in all models when compared to the femur alone model.

The force per unit area calculations demonstrate that in the ASD and FEA modeling, the femur alone model carries 23 times the force per unit area than the implant models but transfers only 30% and 70% of the input force to the hip joint in the FEA and ASD testing, respectively. When comparing this to the implants in either testing system, the presence of an implant significantly increases the force carried by the femur while reducing the force per unit area by 23 times to that of the femur alone model (Fig. 8). All values are statistically significant with three (3) degrees of separation between implant and femur only models (Table V).

The FEA modeling demonstrated a near elimination of the NCF, shear and stress forces on the lateral tissues of the simulated stump-socket interface with a shifting of these forces to the weight-bearing distal stump (Fig. 4A–D and Tables IVA and IVB). The shifting of shear forces is best depicted in comparing the shift of location of the area under the colored lines in Figure 4A, Model-1, Sub-models "a," "b," "c," and "d" and Figure 4B, Model-2, Sub-model "a," "b," "c," and "d." The shifting of NCF is similarly depicted in Figure 4C, Model-1, Sub-model "a," "b," "c," and "d" and Figure 4D Model-2, Sub-model "a," "b," "c," and "d." The significant shift in location of the greater area demonstrates the downward shift of these forces.

DISCUSSION

The purpose of this study was to test the hypothesis: "A properly designed implant that harnesses the principle of the incompressibility of fluids can improve the weight carrying

Downloaded from https://academic.oup.com/milmed/article-abstract/184/supplement_1/627/5418698 by University of Florida user on 02 April 2019

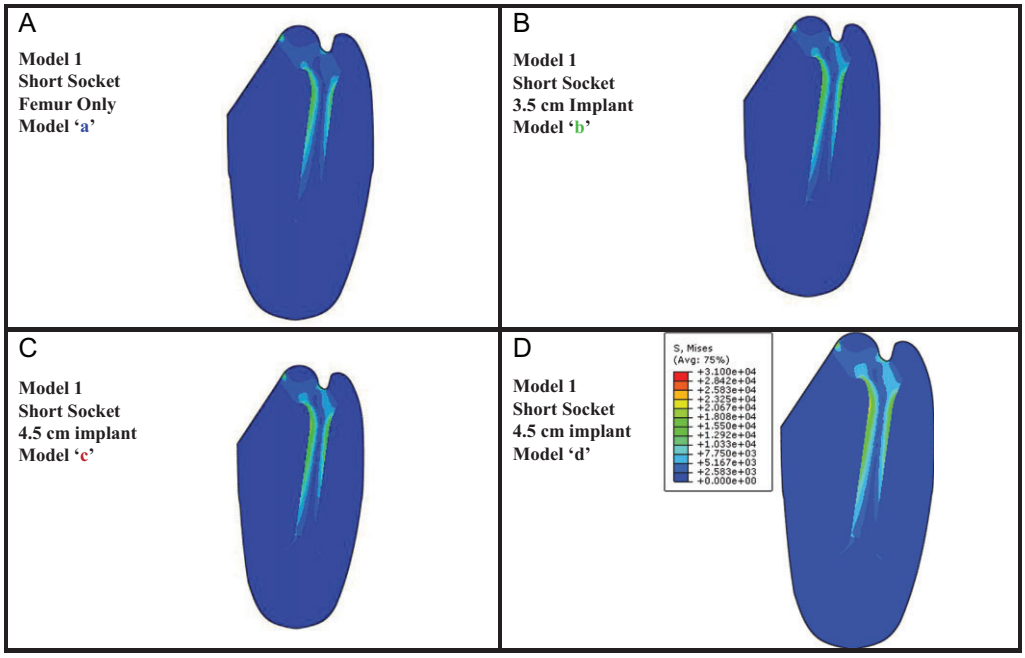

FIGURE 5. Von Mises stress transferred to femur in FEA Model 1 Short Socket Subtypes "a", "b", "c", and "d" (See Figs 2 and 3). Data demonstrate that as implant size increases to the 4.5 cm implant there is more force transferred to and carried by the femur to greater than 90% of maximum applied input force (Kg). The femur alone model carried only 30% of the maximum applied input force. These data demonstrate that the hip joint would be near fully loaded with marked reduction in force per unit area on the stump tissue (see Fig. 8).

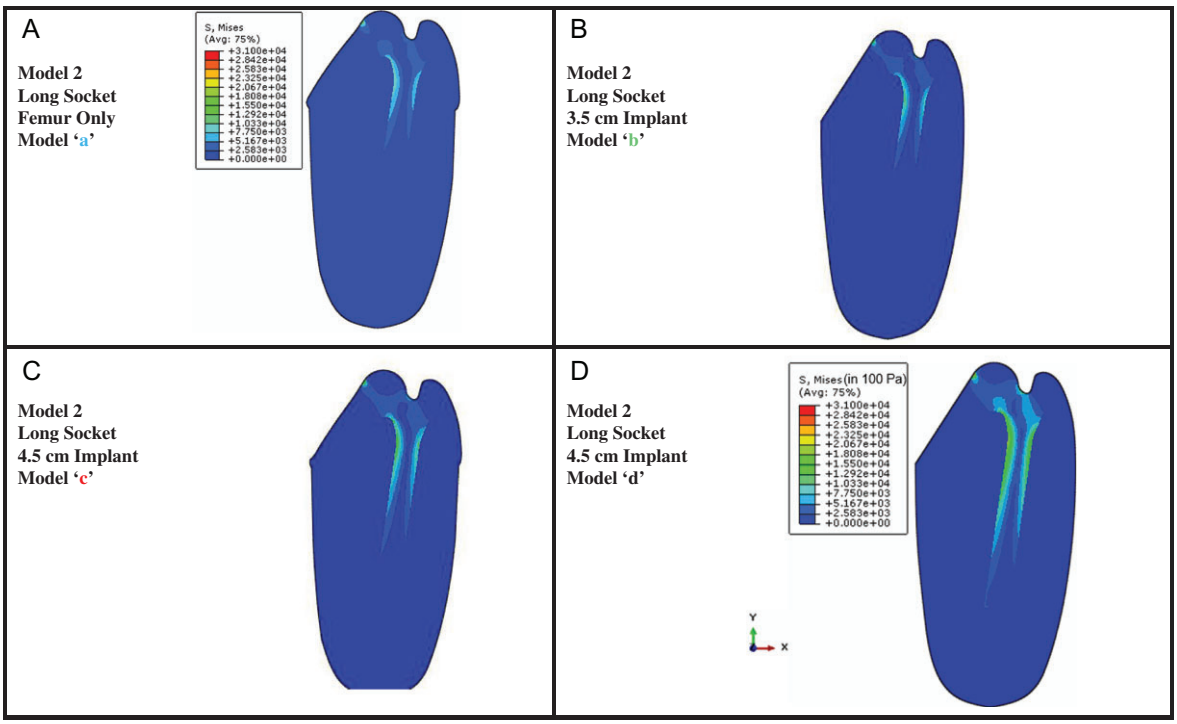

FIGURE 6. Von Mises stress transferred to femur in FEA model 2 long socket subtypes "a", "b", "c", and "d" (see Figs 2 and 3). Data demonstrate that as implant size increases to the 4.5 cm implant there is more force transferred to and carried by the femur to greater than 90% of maximum applied input force (Kg). The femur alone model carried only 30% of the maximum applied input force. These data demonstrate that the hip joint would be near fully loaded with marked reduction in force per unit area on the stump tissue (See Fig. 7).

Downloaded from https://academic.oup.com/milmed/article-abstract/184/supplement_1/627/5418698 by University of Florida user on 02 April 2019

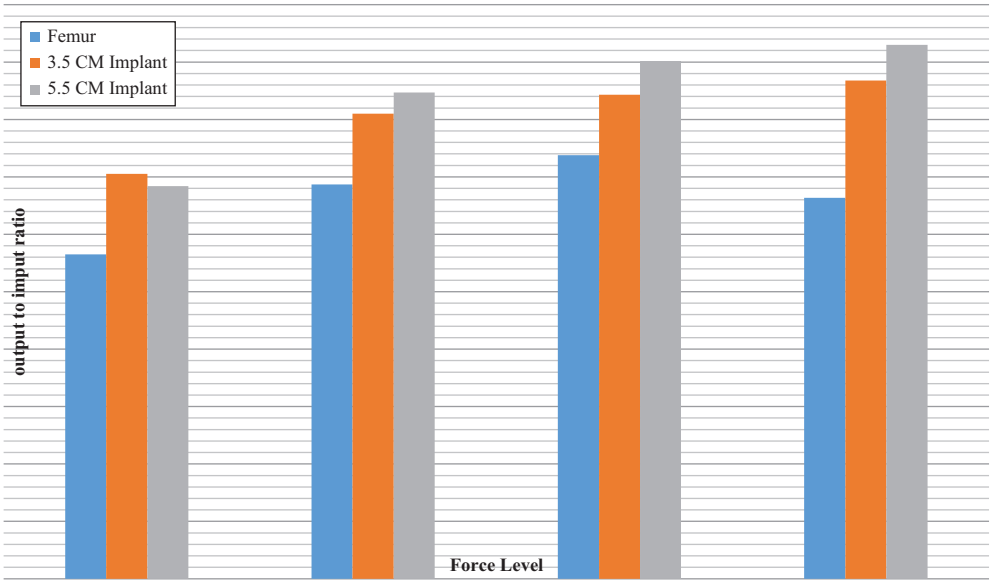

FIGURE 7. Graph demonstrates progressive increase in Output Force recorded at proximal fixation point of ASD as size of implant increases along with increase in surface area. "Y" axis output to input ratio. "X" axis force input levels (applied in Kg). Gray 5.5 cm diameter implant, Copper 3.5 cm diameter implant, Blue 1.5 cm Femur diameter only.

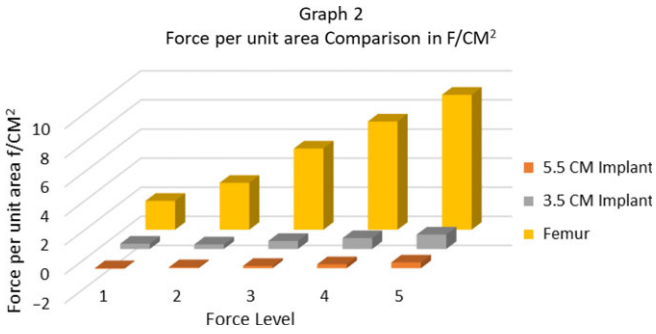

FIGURE 8. FORCE per UNIT AREA. Graph demonstrates increase in force per unit area (Kg/cm^2) as implant size decreases with femur alone carrying a large force per small area but only transmits a small ratio of applied force. "Y" axis force per unit area Kg/cm^2. "X" axis force level, Force applied in Kg. Copper-5.5 cm diameter implant, Gray-3.5 cm diameter implant, Gold-1.5 cm Femur diameter only.

ability of an amputee's residual femur and reduce the frictional forces at the stump external socket interface." Both the FEA and ASD data support the hypothesis with correlation between the ASD and the FEA result. Both systems reported a high transfer of applied force to the simulated femur when the prototype implants were used in the testing. The maximum percentages of force recorded in the femur and proximal hip were 93% and 90% for ASD and FEA simulation, respectively. The data indicate that the ASD and FEA results parallel each other (ASD Table IIA, Table V, Figure 7, and FEA Figs 5A–D and 6A–D). Both systems demonstrated a low transfer of force to the femur in the femur alone models.

Limitations include the reality that the proposed implant may not respond *in vivo* exactly the same as measured in the *in vitro* modeling suggests. Additionally, FEA design parameters and boundary conditions cannot account for scaring and loss of muscle function and mass which may impact *in vivo* function of the implant. To control for this, the FEA's modeling design of the various tissues was based on Young's modulus and Poisson ratios typically found in the human body (Table I).[35–43] The ASD testing used FBI ballistic get to simulate human tissue.

The ASD data (Fig. 8) demonstrate a marked reduction in force per unit area as the size of the implant increases. This distribution and collection of force over a larger surface area allow for the principle of fluid incompressibility to transmit more of the force to the simulated femur (ASD Table IIB, Fig. 7). The FEA Von Mises stress calculations and figures support this observation (Figs 5A–D and 6A–D).

Additional benefits noted was that the FEA calculations revealed that the NCF and shear forces that are present at the stump-socket interface are negated and transferred to the distal weight-bearing end of the stump when a prototype implant is present. This is important as it unloads the lateral skin of the femur and reduces the force per unit area on the distal stump while increasing the available area of force collection. With the femur alone model, the frictional and shear forces remain localized along the lateral edges of the stump (Fig. 4A–D).

CONCLUSIONS

In this study, ASD and FEA modeling validated the proposed hypothesis that a properly designed innovative medical implant that harnesses the principles of fluid incompressibility can increase the weight carrying of the residual femur and reduced the frictional and stress forces on the residual amputee stump. *With implant* attached to the femur, the FEA and ASD femurs carried 90% and 93% respectively of the force of walking.

Downloaded from https://academic.oup.com/milmed/article-abstract/184/supplement_1/627/5418698 by University of Florida user on 02 April 2019

TABLE V. Calculations Is True or False for Three (3) Degrees Separation Between Femur, 3.5in Implant and 5.5in Implant

Force Level	Femur Only	Force Level	Femur vs 3.5 cm	Femur vs 5.5 cm	Force Level	3.5 cm Output	Force Level	3.5 cm vs 5.5 cm	Force Level	5.5 cm Output
0 vs 1	True	1 vs 1	True	True	0 vs 1	True	1 vs 1	True	0 vs 1	True
1 vs 2	True	2 vs 2	True	True	1 vs 2	True	2 vs 2	True	1 vs 2	True
2 vs 3	True	3 vs 3	True	True	2 vs 3	True	3 vs 3	True	2 vs 3	True
3 vs 4	True	4 vs 4	True	True	3 vs 4	True	4 vs 4	True	3 vs 4	True

99% confidence interval on statistical significance of separation.
Formula ($\mu1 + 3*\delta1) < (\mu2 - 3*\delta2$).

Without implant, the FEA model and ASD femur carried only 35% and 77%, respectively, of the force or weight of walking (Table V). Figure 4a–d from the FEA modeling demonstrates that the normal contact forces and shear forces are pushed the distal weight-bearing area of the amputee stump, relieving the lateral stump of frictional forces. The ASD mechanical testing support and parallel the FEA modeling with both systems supporting the hypotheses with confidence intervals of three sigma separation between implant and no implant models.

PREVIOUS PRESENTATIONS

2017 MHSRS Poster Presentation, Gaylord Hotel MHSRS Meeting, Orlando, Florida. Abstract ID MHSRS-17-0008. Poster ID #363 Orthotics and Prosthetics. Presented: Monday August 28, 2017.

FUNDING

M:14;22-33, LLC Private company. Funding for the FEA modeling was provided by M:14;22-33, LLC through the University of Florida and the Department of Aerospace Engineering. This supplement was sponsored by the Office of the Secretary of Defense for Health Affairs.

ACKNOWLEDGMENTS

Dr Nam Ho Kim, PhD and Tejas Chillale, MS and the University of Florida Department of Aerospace Engineering. I have obtained written permission from all persons named in the Acknowledgments.

REFERENCES

1. Holzer LA, Sevelda F, Fraberger G, Bluder O, Kickinger W, Holzer G: Body image and self-esteem in lower-limb amputees. PLoS One 2014; 9(3): e92943.
2. Sinha R, van den Heuvel WJA, Arokiasamy P: Factors affecting quality of life in lower limb amputees. Prosthet Orthot Int 2017; 35(1): 90–6.
3. Dillingham TR, Pezzin LE, MacKenzie EJ: Use and satisfaction with prosthetic devices among persons with trauma-related amputations: a long-term outcome study. Am J Phys Med Rehabil 2001; 80: 563–71.
4. Meulenbelt HEJ, Dijkstra PU, Jonkman MF, Geertzen JHB: Skin problems in lower limb amputees: a systematic review. Disabil Rehabil 2009; 28(10): 603–8.
5. Evrivades D, Jeffery S, Cubinson T, Lawton G, Gill M, Mortiboy D: Shaping the military wound: issues surrounding the reconstruction at the Royal Centre for Defence Medicine. Philos Trans R Soc Lond B Biol Sci 2011; 366(1562): 219–30.
6. Sapin E, Goujin H, De Almeida F, Fodé P, Lavaste F: Functional gait analysis of trans-femoral amputees using two different single-axis prosthetic knees with hydraulic swing-phase control: kinematic and kinetic comparison of two prosthetic knees. Prosthet Orthot Int 2008; 32(2): 201–18.
7. Fossard L, Cheze L, Dumas R: Dynamic input to determine hip joint moments, power and work on the prosthetic limb of transfemoral amputees: ground reaction vs knee reaction. Prosthet Orthot Intl 2011; 35(2): 140–9.
8. El-Sayed AM, Hamzaid NA, Abu Osman NA: Piezoelectric bimorphs' characteristics as in-socket sensors for transfemoral amputees. Sensors 2014; 14(12): 23724–41.
9. Vrieling AH, Van Keeken HG, Schoppen T, et al: Gait initiation in lower limb amputees. Gait and Posture 2008; 27(3): 423–30.
10. White F. M: Fluid Mechanics, 3rd Ed., New York, McGraw-Hill, 1994.
11. Je´quier E., Constant F: Water as an essential nutrient: the physiological basis of hydration. Eur J Clin Nutr 2010; 64: 115–123.
12. Zachariah SG, Sanders JE: Interface mechanics in lower-limb external prosthetics: a review of finite element models. IEEE Trans Rehabil Eng 1996; 4(4): 288–302.
13. Vannah WM, Childress DS: Modelling the mechanics of narrowly contained soft tissues: the effects of specification of Poisson's Ratio. J Rehabil Res Dev 1993; 30(2): 205–9.
14. Sanders JE, Daly CH: Normal and shear stresses on a residual limb in a prosthetic socket during ambulation: comparison of finite element results with experimental measurement. J Rehabil Res Dev 1993; 30(2): 191–04.
15. Zhang M, Mak AFT, Roberts VC: Finite element modeling of a residual lower-limb in a prosthetic socket: a survey of the development in the first decade. Med Eng Phys 1998; 20(5): 360–73.
16. Schwarze M, Hurschler C, Seehaus F, Oehler S, Welke B: Loads on the prosthesis–socket interface of above-knee amputees during normal gait: validation of a multi-body simulation. J Biomech 2013; 46(6): 1201–6.
17. Dickinson AS, Steer JW, Worsley PR: Finite element analysis of the amputated lower limb: a systematic review and recommendations. Med Eng Phys 2017; 43: 1–18.
18. Smith LN: Implantable prosthetic device for distribution of weight on amputated limb and method of use with an external prosthetic device. US Patent US8882851 B2, vol. filed Sep 20, 2011, issued November 11, 2014.
19. Bae TS, Choi K, Hong D, Mun M: Dynamic analysis of above-knee amputation gait. Clin Biomech 2007; 22(5): 557–66.
20. Surapureddy R: Predicting pressure distribution between transfemoral prosthetic socket and residual limb using finite element analysis. UNF Thesis and Dissertations 2014; 551.
21. Taun LV, Yamamoto S, Hanafusa A: Finite element analysis for quantitative transfemoral prosthesis socket for standing posture. Int J Comput Appl 2017; 170(1): 1–5.
22. Dickinson AS, Steer JW, Worsley PR: Finite element analysis of the amputated lower limb: a systematic review and recommendations. Med Eng Phys 2017; 43: 1–18.
23. Dumas R., Cheze L, Frossard L: Loading applied on prosthetic knee of Transfemoral amputee: comparison of inverse dynamics and direct measurements. Gait Posture 2009; 30: 560–2.

Downloaded from https://academic.oup.com/milmed/article-abstract/184/supplement_1/627/5418698 by University of Florida user on 02 April 2019

24. Ramirez JF, Vélez JA: Incidence of the boundary condition between bone and soft tissue in a finite element model of a Transfemoral amputee. Prosthet Orthot Int 2012; 36(4): 405–14.
25. Mak AF, Zhang M, Boone DA: State-of-the-art research in lower-limb prosthetic biomechanics-socket interface. J Rehabil Res Dev 2001; 38(2): 161–74.
26. Ramírez JF, Muñoz EJ, Vélez JA: Algorithm for the prediction of the reactive forces developed in the socket of transfemoral amputees. Dyna 2012; 79(173): 89–95.
27. Vannah WM, Childress DS: Modelling the mechanics of narrowly contained soft tissues: the effects of specification of Poisson's ratio. J Rehabil Res Dev 1993; 30(2): 205–9.
28. Brennan JM, Childress DS: Finite element and experimental investigation of above knee amputee limb/prosthesis systems: a comparative study. Advances in Bioengineering, ASME Winter Annual Meeting 1991;20:547–50.
29. Sanders JE, Daly CH: Normal and shear stresses on a residual limb in a prosthetic socket during ambulation: comparison of finite element results with experimental measurement. J Rehabil Res Dev 1993; 30(2): 191–204.
30. Modenese L, Phillips AT, Bull AM: An open source lower limb model: hip joint validation. J Biomech 2011; 44(12): 2185–93.
31. Zheng YP, Mak A, Leung AK: State of the art methods for geometric and biomechanical assessment of residual limbs: a review. J Rehabil Res Dev 2001; 38(5): 487–504.
32. Sanders JE, Daly CH: Normal and shear stresses on a residual limb in a prosthetic socket during ambulation: comparison of finite element results with experimental measurement. J Rehabil Res Dev 1993; 30(2): 191–204.
33. Kim NH: Introduction to Nonlinear Finite Element Analysis. New York, NY, Springer, 2015.
34. Gholizadeh H, Osman NAA, Eshraghi A, Arifin N, Chung TY: A comparison of pressure distributions between two types of sockets in a bulbous stump. Prosthet Orthot Int 2015; 40(4): 509–16.
35. Hwang M, Berceli SA, Garbey M, Kim NH, Tran-Son-Tay R: The dynamics of vein graft modelling induced by hemodynamic forces: a mathematical model. Biomech Model Mechanobiol 2011; 11(3–4): 411–23. DOI:10.1007/s10237-011-0321-3.
36. Thanoon D, Garbey M, Kim NH, Bass B: A computational framework for breast surgery: Application to breast conserving therapy. In: Computational Surgery and Dual Training, pp 249–68. Edited by Garbey M, Bass BL, Collet C, Mathelin M, Tran-Son-Tay R NY, Springer, 2010.
37. Bei Y, Fregly BJ, Sawyer WG, Banks SA, Kim NH: The relationship between contact pressure, insert thickness, and mild wear in total knee replacements. Comput Model Eng Sci 2004; 6(2): 145–52.
38. Avril S, Bouten L, Dubuis L, Drapier S, Pouget J-F: Mixed experimental and numerical approach for characterizing the biomechanical response of the human leg under elastic compression. J Biomech Eng 2010; 132(3): 031006.
39. Dubuis L, Avril S, Debayle J, Badel P: Identification of the material parameters of soft tissues in the compressed leg. Computer Methods in Biomechanics and Biomedical Engineering, Informa. Healthcare 2012; 15(1): 3–11.
40. Rho JY, Ashman RB, Turner CH: Young's modulus of trabecular and cortical bone material: Ultrasonic and micro-tensile measurements. J Biomech 1993; 26(2): 111–9.
41. Zheng Y, Mak AFT: Effective Elastic Properties for Lower Limb Soft Tissues from Manual Indentation Experiment. IEEE Trans Rehabil Eng 1999; 7(3): 257–67.
42. Jing LP, Zeng BX, Zhou Y: China Comparison of isotropic and orthotropic material property assignments on femoral finite element models under two loading conditions. Med Eng Phys 2006; 28(3): 227–33.
43. Mak AFT, Zhang M, Boone DA: State-of-the-art research in lower-limb prosthetic biomechanics socket interface: a review. J Rehabil Res Dev 2001; 38(2): 161–74.

Downloaded from https://academic.oup.com/milmed/article-abstract/184/supplement_1/627/5418698 by University of Florida user on 02 April 2019